Non-nitrogen Doped and Non-metal Oxygen Reduction Electrocatalysts based on Carbon Nanotubes: Mechanism and Origin of ORR Activity

Journal:	*Energy & Environmental Science*
Manuscript ID:	EE-ART-11-2013-043743.R2
Article Type:	Paper
Date Submitted by the Author:	22-Feb-2014
Complete List of Authors:	Waki, Keiko; Tokyo Institute of Technology, Energy Sciences Wong, Raymond; Tokyo Institute of Technology, Energy Sciences Oktaviano, Haryo; Tokyo Institute of Technology, Energy Sciences Takuya, Fujio; Tokyo Institute of Technology, Energy Sciences Nagai, Takuro; National Institute for Materials Science, Kimoto, Koji; National Institute for Materials Science, Yamada, Koichi; Japan Science and Technology Agency,

Table of Contents Graphic

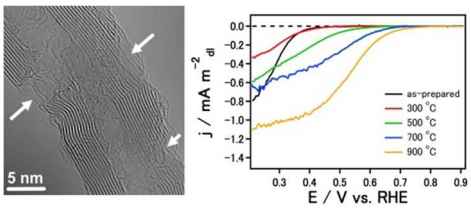

The proposed origin of the improved ORR activity in non-nitrogen doped and non-metal carbon based electrocatalysts is unlikely to be residual metal impurities but from the creation of topological defects caused by the removal of high temperature CO desorbing oxygen functional groups.

Journal Name

RSCPublishing

ARTICLE

Non-nitrogen Doped and Non-metal Oxygen Reduction Electrocatalysts based on Carbon Nanotubes: Mechanism and Origin of ORR Activity

Cite this: DOI: 10.1039/x0xx00000x

Received ooth January 2012,
Accepted ooth January 2012

DOI: 10.1039/x0xx00000x

www.rsc.org/

Keiko Waki,[*,†,‡] Raymond A. Wong,[†] Haryo S. Oktaviano,[†] Takuya Fujio,[†] Takuro Nagai,[§] Koji Kimoto[§] and Koichi Yamada[‡]

We show high activity in non-nitrogen doped and non-metal electrocatalysts based on carbon nanotubes with onset potential up to 0.73 V vs. RHE by the formation of hole defects on the wall of carbon nanotubes, followed with annealing under Ar atmosphere. From the power generation test, this catalyst can deliver maximum output power of 55.68 mW(mg-CNT cathode)$^{-1}$. Through temperature programmed desorption (TPD) and electrochemical analysis, the creation of new active sites are correlated with the removal of high temperature CO desorbing functionalities. Residual metal impurities were examined by the use of inductively coupled plasma-mass spectroscopy (ICP-MS), high angle annular dark-field (HAADF) and electron energy loss (EELS) analysis. The extremely low amount of metal impurities and the absence of impurity coordination at the edge planes after electrochemical characterizations suggest that it is unlikely that impurities directly contribute to ORR. We conclude by proposing that the origin of ORR activity is a result of carbon restructuring and the possible formation of topological defects caused during the removal of high temperature CO desorbing functional groups.

Broader context

Tremendous investigations have been carried out to exploit the distinctive features of carbon nanotubes for renewable energy applications including fuel cells and metal-air batteries. Although carbon nanotubes themselves are considered to be inactive for oxygen reduction reaction (ORR), the inclusion of nitrogen doping and the formation of metal-nitrogen-carbon complexes have been shown to exhibit high ORR activity. Here, we show alternative ORR electrocatalysts without any additives, not only noble metals, but also non-noble metals and nitrogen, namely, purely made of carbon nanotubes in which defective holes can form from the outer walls to the center of nanotubes. We conclude that it is unlikely that impurities directly contribute to ORR and propose that the removal of high temperature CO desorbing functional groups in the defect hole vicinities coinciding with carbon restructuring can result in topological defects which is a possible explanation for the high ORR activity. This work opens the door in realizing high-performance fuel cells through the design of pure carbon-based catalysts.

Introduction

Intensive research efforts have been directed towards the cost reduction of fuel cells through the development of non-noble metal catalysts for the electrochemical reduction of oxygen. In the past few decades, metal-free catalysts and non-noble catalysts involving nitrogen and transition metal doping have gained popularity among researchers as possible alternatives to the conventional platinum based cathode catalyst.[1-9] Early work began with macrocycles containing transition metals and nitrogen coordinated with carbon.[2,3] Later it was found that combination of transition metal, carbon support, nitrogen, and high temperature annealing are essential for durable and active oxygen reduction reaction (ORR) catalysts.[1,2] Examples include the pyrolysis of transition metal macrocycles,[2] nitrogen doping through high temperature

annealing in NH_3,[2,6] or the sputtering of Metal-C-N thin films followed by heat treatment.[7]

New approaches using nano-carbon materials as the active catalyst material have also been investigated. In alkaline media, these so-called "metal-free catalysts", nitrogen-doping is recognized as the key factor for improved ORR activity and any metals, if present, are considered as impurities.[8,9] The introduction of nitrogen atoms are believed to create net positive charge on the adjacent carbon atoms in the carbon nanotube plane, resulting in the charge-induced favorable O_2 adsorption and charge transfer.[9]

In acid media it has been suggested that since nitrogen containing carbon nanostructures retain most of their ORR activity even after the removal of its metal components, metal species may not be the direct active sites,[4,10] but may play a role in the formation of a special type of carbon that is catalytically active towards ORR.[2] However, Dai and coworkers recently reported exceptionally high ORR activity in acid by unique oxidation of the outer walls to partially unzip few-walled carbon nanotubes followed by nitrogen doping by high temperature NH_3 annealing.[6] For this nitrogen-doped nanotube-graphene catalyst, it was concluded that nitrogen (5.3 at%) doping and Fe impurities (0.24 at%) are essential in forming Fe-N-C which is believed to be the active centers for ORR. Additionally, various pristine carbons have been examined on their intrinsic structural properties as a host for Fe/N/C catalytic sites giving the indications that smaller diameter, higher disordered phase and larger graphene layers are important for improved performance.[11]

However, the nature of carbon materials itself as the catalyst material did not attract attention as it was considered that edge plane exposure alone, without nitrogen doping, did not lead to improved ORR activity in acidic electrolytes.[12-14] More than ten years ago, molecular dynamics (MD) simulations suggested that topological defects in the form of pentagon-heptagon defect pairs can enhance the activation behavior of ORR,[15] and this has been experimentally supported by our previous work.[16] However, conclusions are always obscured by the existence of impurities in carbon and by the variation in carbon nanomaterials with respect to synthesis procedures, defects, and morphology.[12,14]

Previously, we have found that after the removal of functional groups in functionalized hollow MWNTs, the onset potential shifted to the positive direction up to 0.55 V vs. RHE.[17] This result suggested that functional groups themselves are not responsible for such enhancement of ORR catalyst performance. However, the nature of the active site has not been well investigated.

Herein, we show high activity in non-nitrogen doped and non-metal carbon based catalysts by investigating the origin of ORR activity through the evaluation of functional groups and structural morphology of multi-walled carbon nanotubes (MWNTs). The distribution of oxygen functional groups and structural morphology of the MWNTs are modified by chemically drilling the MWNT walls[18,19] as a method for creating edge and hole defects, followed by acid washing. The drilling method uses cobalt oxide as a low temperature carbon oxidation catalyst which allows for high edge and hole defect concentration and maintains high conductivity and crystallinity in the intact areas. The removal of oxygen functionalities by annealing in Ar atmosphere showed an improvement of ORR activity and onset potential of ~0.73 V vs. RHE. Through temperature programmed desorption (TPD) and electrochemical analysis, the new active sites are correlated with the high temperature CO desorption functionalities and the resulting morphological changes. Residual metal impurities were examined by the use of inductively coupled plasma-mass spectroscopy (ICP-MS), high angle annular dark-field (HAADF) and electron energy loss (EELS) analysis. The extremely low amount of metal impurities and the absence of impurity coordination at the edge planes after electrochemical characterizations suggest that it is unlikely that impurities directly contribute to ORR.

Experimental

Material synthesis

The hollow multi-walled carbon nanotubes (MWNTs) used was provided by Showa Denko KK, Japan (VGFX-XA, diameter: 15 nm, approximate length: 1 μm; containing Fe impurities < 1 wt%). As a precursor, functionalized MWNTs (PMWNTs) were obtained by annealing pristine MWNTs in air at 500°C to remove amorphous carbon, followed by reflux in 2 M sulfuric acid and concentrated nitric acid (1:1 v/v) for 4 h. This was followed by filtration with deionized water and drying overnight. Chemically drilled, defective MWNTs were prepared by first impregnating the prepared functionalized MWNTs with 10 wt% Co, dispersed in ethanol. Chemically drilled, defective MWNTs were synthesized by either oxidizing the Co impregnated PMWNT under air atmosphere at 250°C for 25 minutes or first under Ar atmosphere at 300°C for 3 h followed by oxidation in air at 250°C for 25 minutes. After air-oxidation, the cobalt oxides were removed by acid washing in concentrated nitric acid at 120°C for 1h (DMWNT-HNO_3), or 2 M sulfuric acid at room temperature for 4 h (DMWNT-H_2SO_4) followed by filtration with deionized water and drying overnight. Self-standing buckypaper was fabricated from PMWNT, DMWNT-HNO_3, and DMWNT-H_2SO_4. Typically, 25 mg of PMWNT, DMWNT-HNO_3, or DMWNT-H_2SO_4, 1 mL Triton X-100 surfactant, 5 mL 1-propanol, and 100 mL of deionized water (~18 MΩ) was mixed thoroughly by the use of a homogenizer. The mixture was then filtered through 0.45 μm pore size mixed cellulose ester membrane followed by the addition of 400 mL deionized water and 100 mL of 2-propanol. The buckypaper samples were dried overnight in a drying oven at 60°C and then subsequently peeled off (Fig. S1). For annealing, the buckypaper samples were annealed in flowing Ar for 1h at their respective temperatures.

Electrochemical characterizations

All the electrochemical measurements were done at room temperature (25˚C). The electrolyte used was 0.1 M $HClO_4$. Typically, the as-prepared buckypaper was cut into 0.5 cm×0.5 cm pieces which has a typical mass of ~0.5mg and was sandwiched in between two glassy carbon plates secured by two PTFE nuts and bolts and used as the working electrode (Fig. S2). Half of the buckypaper was fixed to the glassy carbon plates and half was in contact with the electrolyte. The reference electrode employed was a saturated Ag/AgCl electrode and the counter electrode was a platinum mesh. All the data in this work is presented with respect to the reversible hydrogen electrode (RHE). The scan rate employed for all the measurements was typically 1 mV/s. Prior to the electrochemical measurements Ar or O_2 was bubbled for at least 30 minutes to ensure saturation. The durability test was done by cycling under saturated O_2 for 8000 cycles with a scan rate of 50 mV/s and voltage window [0.2 - 0.6] V vs. Ag/AgCl. The single cell test consisted of an anode catalyst loading of 1 mg cm^{-2} of Pt/C (70 wt%). The cathode consisted of DMWNT-H_2SO_4 heat treated (Ar 900˚C) and Nafion as a binder giving a catalyst loading of 1.85 mg cm^{-2}. The area of the cell was 5 cm^2.The cell temperature was 90˚C, anode gas: pure hydrogen (200 sccm, 0.3 MPa), cathode gas: pure oxygen (400 sccm, 0.3 MPa) under 100% humidity.

Characterization

The oxygen functional groups were evaluated with the use of temperature programmed desorption (TPD) (ESCO, EMD-WA1000S) containing a quadrupole mass spectrometer system (QMG 422) for analyzing the desorbed gases. The buckypaper samples were heated via infrared lamp to 1100˚C at a constant rate of 30˚C/min under ultra-high vacuum conditions with a base pressure of $2.0x10^{-7}$ Pa. N_2 adsorption-desorption were measured at 77 K on a BEL Japan, BELSORP-mini II instrument. The MWNT samples were degassed at 120 °C under vacuum for 3h, prior to the measurement. The ICP-MS data was obtained by using Shimadzu ICPS-8100. The buckypaper samples were first calcined at 800˚C and the residues were dissolved in 2 mL concentrated HNO_3 and then diluted to 10 mL for measurement. The sample DMWNT-H_2SO_4-Ar900 (after electrochemical measurements) consisted of CV measurements of 6 cycles at 2 mV/s under saturated Ar, followed by 3 cycles at 1 mV/s under saturated Ar, and finally followed by 3 cycles at 1 mV/s under saturated O_2 conditions. There was no noticeable change in ORR activity before or after electrochemical characterizations. The Monochromated TEM imaging was performed at the National Institute of Materials Science (NIMS) using TEM (FEI Titan Cubed) operated at an acceleration voltage of 80 kV with a monochromator and a spherical aberration corrector (CEOS, CETCOR). The high-angle annular dark field (HAADF) imaging was carried out using the microscope operated at 80 kV in the scanning electron microscopy (STEM) mode with a spherical aberration corrector (CEOS GmbH, DCOR). The EEL spectra were obtained in STEM mode with the use of the electron loss spectrometer (Gatan Inc., GIF Quantum 966) at a collection semi-angle of 80 mrad.

Results and discussion

As a precursor, pristine MWNTs (VGCFX-XA) were first functionalized by heat treating in air followed by reflux in concentrated nitric acid and 2 M sulfuric acid (1:1 v/v) for 4 h (PMWNT). In this study, pristine (raw) MWNTs were avoided to be used as the precursor, because they contain large amounts of impurities that can obscure the ORR investigation. Similar to our previous work regarding chemically drilled and defective carbon nanotubes,[18,19] the precursor was then impregnated with cobalt followed by low temperature carbon oxidation via solid state reaction at 250°C for 25 minutes in air. Following chemical drilling, the cobalt oxides were removed by acid washing in boiling concentrated nitric acid (DMWNT-HNO_3) for 1 h or 2 M sulfuric acid (DMWNT-H_2SO_4) at room temperature for 4 h. Transmission electron micrographs (TEM) of the as-prepared samples are shown in Fig. S3.

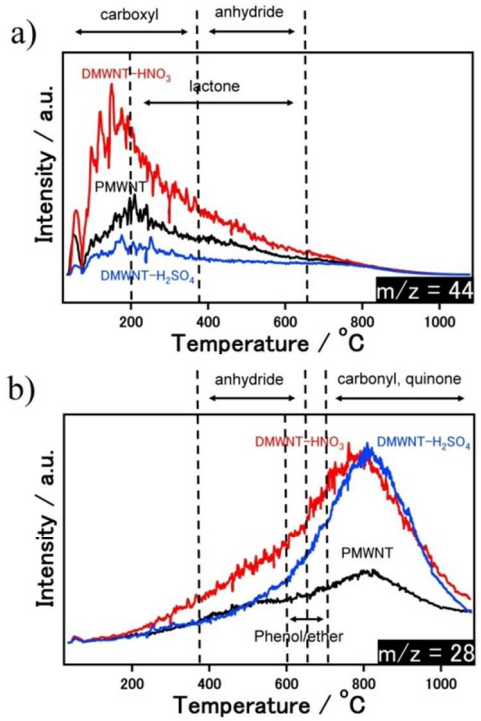

Fig. 1 Temperature programmed desorption (TPD) spectra (a) CO_2 desorption (b) CO desorption of precursor (PMWNT) to chemical drilling, chemically drilled MWNT washed by nitric acid (DMWNT-HNO_3), and drilled MWNT washed by sulfuric acid (DMWNT-H_2SO_4). The dotted lines indicate desorption temperature ranges of as-mentioned O-functionalities.[18,20,21]

TPD analysis under ultra-high vacuum (UHV) conditions was done to correlate the role of functional groups and ORR activity of the MWNT samples. TPD can uncover qualitative and quantitative information regarding the identity of surface functional groups which decompose at different temperature

ranges, while releasing CO, CO_2 and water.[18,20,21] Typically in carbon materials, phenols, carbonyls, quinones, and pyrone groups release CO, while lactones and carboxylic acids release CO_2 during annealing[18,20,21]. Carboxylic anhydrides are an exception as they desorb both CO and CO_2.[18,20,21] The TPD results (Fig. 1) indicate that the low temperature (<400°C) desorbed CO_2 (Fig. 1a) shows evidence for the presence of carboxyl-based functional groups. DMWNT-HNO_3 contains the higher concentration of low temperature CO_2 desorbed functional groups. These results are reasonable as nitric acid used in the removal of cobalt oxide for DMWNT-HNO_3 is known to introduce carboxyl-based functional groups.[13] Regarding the CO desorption spectra (Fig. 1b), DMWNT-HNO_3 and DMWNT-H_2SO_4 show similar desorption profiles. The majority of the CO desorbed for the samples are in the high temperature region, peaking at ~800°C, which strongly indicates the presence of quinone, carbonyl, and/or pyrone based functional groups. The oxygen content was also determined quantitatively (supplementary information Table S1) based on the amount of CO and CO_2 desorbed and was found to be 4.38, 9.53 and 5.30 at% for PMWNT, DMWNT-HNO_3, and DMWNT-H_2SO_4 respectively, indicating that hole defect fabrication and acid washing introduces oxygen functionalities. Overall, there is a close relationship between the degree of defect formation and the amount of CO and CO_2 desorbed, as annealing is accompanied by a loss of carbon by gasification of the carbon nanotube structure. Also, oxygen functionalities reside along edges planes and the surface of the tube walls, and thus, higher amounts of CO/CO_2 desorption indicates a higher density of edge plane and hole defects.

X-ray photoelectron spectroscopy (XPS) analysis was also carried out to study the oxygen functionalities after defect fabrication on MWNTs. As indicated from the XPS survey scan (Fig. S4), DMWNT-HNO_3 has higher oxygen content than that of DMWNT-H_2SO_4. The oxygen content was obtained from high resolution C1s and O1s spectrum (Fig. S5), are 9.24 and 5.28 at% of oxygen for DMWNT-HNO_3 and DMWNT-H_2SO_4, respectively. These results suggest that XPS are in agreement with the quantitative TPD analysis. Attempting to study the defects structure, Raman spectroscopy was conducted. Typical Raman spectrum of MWNTs (Fig. S6) shows two strong peaks at ~1580 and ~1350 $cm^{-1,}$ which corresponds to graphitic carbon peak "G" and disordered carbon peak, "D", respectively. The D-band intensity relative to the G-band (I_D/I_G) is often used as measure of the nanotube quality. The detailed I_D/I_G values for different MWNTs are listed in Table S2 (supplementary information). DMWNT-HNO_3 has the largest I_D/I_G, followed by DMWNT-H_2SO_4 and then pristine MWNTs, indicating that DMWNT-HNO_3 has more disordered structures than that of DMWNT-H_2SO_4. Due to the disordered characteristics, it can be understood that DMWNT-HNO_3 has more O-functionalities than that of DMWNT-H_2SO_4 as indicated from TPD and XPS results.

Nitrogen (N_2) adsorption-desorption was done to evaluate the specific surface area and porosity of DWMNTs. N_2 adsorption-desorption profiles for DMWNTs can be considered as type IV with an obvious hysteresis loop, indicating its mesoporous characteristics (Fig. 2a), and the BJH plot (Fig. 2b) reveals the broad distribution of mesopores. DMWNT-HNO_3 and DMWNT-H_2SO_4 show BET specific surface areas of 326 and 366 m^2/g, respectively. The different packing characteristics of both DMWNTs could be confirmed by the absence of pores with diameters in the range of 10-30 nm (Fig. 2b), suggesting that the packing of DMWNT-H_2SO_4 has a less compact structure than DMWNT-HNO_3, allowing for more N_2 to be adsorbed.

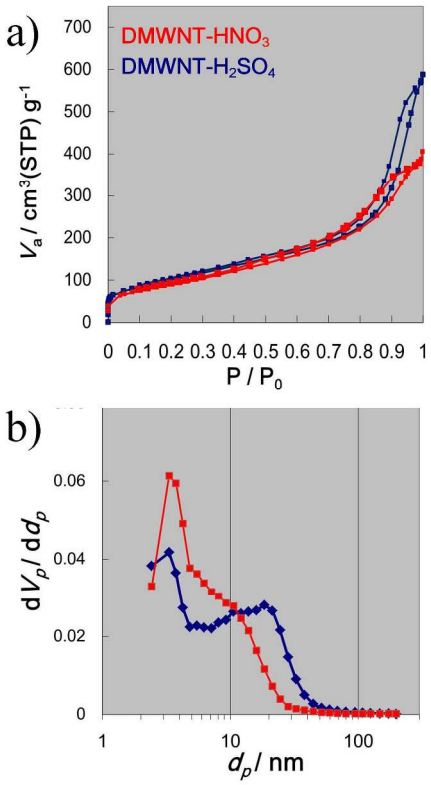

Fig. 2 N_2 adsorption-desorption isotherm of and BJH plot for corresponding DMWNT-HNO_3 and DMWNT-H_2SO_4

For the electrochemical measurements, buckypaper, a free-standing aggregate of carbon nanotubes was fabricated with MWNTs (Fig. S1) from the samples and characterized as the working electrode. Using buckypaper as the working electrode has several benefits including uniform surface structure, and consistent mass loading. Buckypaper also contains sufficiently large mass loading, thus it can be considered that buckypaper can provide a clear evaluation of ORR performance due to the greater number of active sites participating in the electrochemical measurements. Buckypaper also allows for the facile characterization of impurities before and after electrochemical characterizations which will be discussed later. Consequently, in this study, the utilization of buckypaper as an alternative working electrode was used to evaluate the ORR activities associated with the different defective structural morphologies. To avoid differences originating from surface

structure and area, for all of the electrochemical measurements, the current response is normalized to the double layer (dl) electrochemical surface area (supplementary information). Under saturated Ar conditions, two types of capacitance can be visualized. Double layer capacitance is correlated with electrochemical-effective surface area, while the presence of features that deviate from the double layer are known as faradic capacitance that is believed to be related to quinone redox pairs.[22-23] The cyclic voltammetry (CV) curves show the effects of quinone redox in the potential range <0.7 V (Fig. 3), but the current responses appear different despite similar CO profiles as observed by TPD. This suggests that another mechanism is at work. The proposed reason is related to the presence of CO_2 desorbed species, mainly carboxylic acids in DMWNT-HNO_3 which can influence the amount of electrochemically active quinones. This is further exemplified in the ORR activities of DMWNT-HNO_3 and DMWNT-H_2SO_4 for the potential range 0.15-0.4 V (Fig. 3). When carboxyl-based groups are removed in DMWNT-HNO_3 by annealing at 300°C in Ar (Fig. S7), ORR activity is suppressed and more closely resembles DMWNT-H_2SO_4. The presence of carboxyl groups can cause differences in activity through its impact on the electronic structure[24] and consequently influence the wettability and/or the amount of active quinones partaking in the reactions.[22.23]

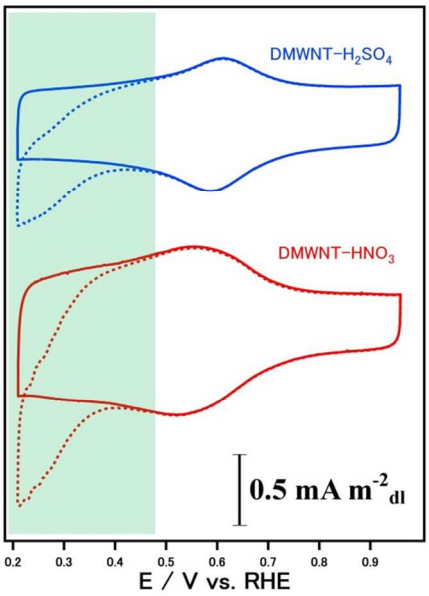

Fig. 3 Cyclic voltammograms of buckypapers fabricated from DMWNT-HNO_3, and DMWNT-H_2SO_4 under saturated Ar (solid) and O_2 (dotted) in 0.1 M $HClO_4$ with scan rate of 1 mV/s. Green section indicates oxygen reduction region.

The effect of the functional group removal towards ORR activity was carried out by annealing at 900°C in Ar. The temperature 900°C was chosen due to the TPD results (Fig. 1) indicating that the majority of oxygen functionalities are removed when 900°C is reached and this is further confirmed by CV in Ar by the absence of faradaic capacitance (Fig. 4a inset). The ORR polarization curve (Fig. 4a) shows that the samples exhibit improved onset potentials of ~0.73 V suggesting the creation of new catalytic sites which is distinctly different from the quinone mediated ORR mechanism discussed earlier.

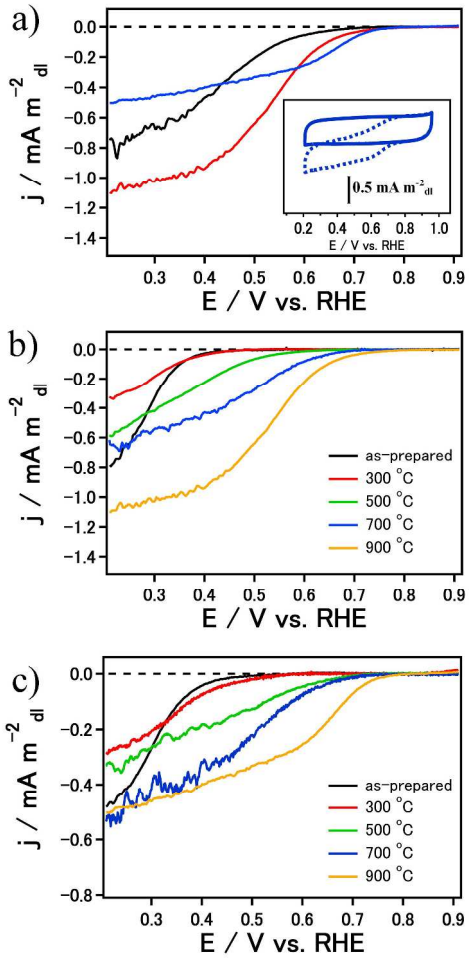

Fig. 4 (a) ORR polarization curves of buckypapers fabricated from the precursor PMWNT (black), DMWNT-HNO_3 (red) and DMWNT-H_2SO_4 (blue) after annealing at 900°C in Ar to remove oxygen functionalities (inset) cyclic voltammetry curve of DMWNT-H_2SO_4 (annealed at 900°C in Ar) in Ar (solid) and O_2 (dotted). ORR polarization curves of (b) DMWNT-HNO_3 and (c) DMWNT-H_2SO_4, showing the effects of increasing annealing temperature. All measurements are conducted in 0.1 M $HClO_4$ with a scan rate of 1 mV/s.

There are however, differences in the potential and rate at which the diffusion limiting current is reached. These results suggest that the removal of functional groups by annealing in Ar is crucial in achieving high activity and differences in the type and distribution of functional groups is related to the formation of defective structures which can strongly influence ORR performance. The apparent difference in diffusion limiting current observed for DMWNT-HNO_3-Ar900 and DMWNT-H_2SO_4-Ar900 can be attributed to the difference of

surface functional groups and the disordered degree of MWNTs that may affect their wettability nature.

With the realization that the removal of oxygen functionalities improves ORR performance, the dependence of ORR activity on annealing temperature for DMWNT-HNO_3 (Fig. 4b) and DMWNT-H_2SO_4 (Fig 4c) was examined. With the annealing treatment of DMWNTs at 300°C, DMWNT-HNO_3-Ar300 and DMWNT-H_2SO_4-Ar300 showed lower current density than that of the as prepared catalysts. This can be explained by the removal of carboxyl groups during the low temperature annealing process (Fig. 1), which can influence the wettability nature and/or the amount of electrochemically active sites. For DMWNTs annealed above 300°C, the ORR onset potential and activity continues to improve with the increase in annealing temperature. For temperatures above 700°C, the onset potentials are similar at ~0.73 V indicating similar catalytic sites (onset potential is defined when the current density is greater than 0.02 mA/m^2_{dl}). Relating to TPD analysis, CO releasing functional groups begin to evolve CO at 500°C and temperatures above 700°C correlates with the removal of quinone-based functionalities.[20,21] The removal of functional groups is confirmed in the TPD spectra of DMWNT-HNO_3 following annealing at 900°C in Ar (Fig. S8), which shows that almost all of the CO releasing functional groups have disappeared. With the realization that the removal of oxygen functionalities improves ORR activity, questions arise about the nature of the disordered edges and surfaces following the removal of oxygen functionalities. The unpaired electrons left after the removal of CO releasing functional groups can result in (1) radicals or dangling bonds, (2) new functionalized sites through the recombination with ambient oxygen and water, (3) the possible formation of pentagon and/or heptagon topological defects through carbon restructuring, and lastly (4) interactions with residual metal impurities forming metal-carbon complexes.

On the edge planes, the formation of radicals and dangling bonds can occur from the removal of functional groups during annealing. However, if there is no steric hindrance effect, the recombination with oxygen or water is favorable for stabilization. In fact, unpaired electrons of the precursor (PMWNT) were characterized by electron spin resonance (ESR) (Fig. S10) and it was found that a small signal could be detected before annealing, but after annealing in Ar at 900°C, no signal could be obtained, indicating that unpaired electrons decreased after the annealing process. In any case, such radicals are not expected to be the active sites for ORR. For nitrogen-doped carbons, the substitution of oxygen with nitrogen, forming pyridinic-N and pyrrolic-N is believed to occur on the edge planes[25,26] and is related to their high ORR activity.[25] In the case without nitrogen, the dangling bonds generated after the removal of functional groups can recombine with oxygen when exposed to air. However, oxygen-containing functional groups that can also form in the drilling and acid washing processes did not lead to high ORR activity. Furthermore, we found that samples annealed in Ar and in ultra-high vacuum show differences in the distribution of oxygen recombination (Fig. S8 and S9) due to differences in the ambient environment oxygen concentrations but this resulted in similar onset potential. This indicates that the recombination of functional groups is unlikely as the source of improvement in ORR activity. We note however, that there is a possibility that any remaining high temperature desorbing functional groups (>900°C) such as pyrones[21], may have a role in the improved ORR activity.

On the other hand, carbon materials often contain arrangements of non-hexagonal carbon atoms.[27,28] For these topological defects, it has been suggested that pentagon-heptagon pair defects[15,16] and the creation of edge plane defects[26,29] can affect the electronic structure in a manner that can assist in electron transfer and improve ORR performance. Potential pentagon/heptagon defects formed from the restructuring of the carbon lattice at elevated annealing temperatures coinciding with the removal of oxygen functional groups is one possible mechanism for the high ORR activity. The removal of high temperature CO desorbing functional groups results in the removal of C atoms directly in the hexagonal rings and this leads to significant alteration of the carbon lattice, but the removal of CO_2 releasing functional groups includes C atoms connected to the hexagonal rings and excludes C atoms directly in the hexagonal rings. This can be seen as there is no improvement in onset potential for DMWNT-HNO_3 sample after annealing at 300°C, but the onset potential improves considerably when annealed above 500°C. Therefore, a possible mechanism for the formation of the active sites is the reconstruction of the C defects occurring from the removal of CO desorbing functional groups. It should be noted that our sample, DMWNT-H_2SO_4, has 5.30 at% of desorbed oxygen containing 4.12 at% of oxygen from CO desorbing functional groups (Table S1), showing that with a relatively low concentration of CO desorbing functional groups, such high ORR performance was attained. The TPD and electrochemical characterizations of precursor (PMWNT) (Fig. 1 and 4a) also support our proposal that the creation of new active sites is correlated with the removal of high temperature CO desorbing functional groups. The results indicate that ORR activity is lower in the case without hole defects and this is due to its lower amount of CO desorbing functional groups in comparison to DMWNT-HNO_3 and DMWNT-H_2SO_4. It is important to note that the concentration of oxygen functionalities (ie. the hole defects) present before annealing is the main factor that determine ORR activity after annealing. However, oxygen functional groups themselves do not directly partake in the highly active ORR reaction. Furthermore, since our structural modification and controlled oxidation method introduces the desired CO desorbing functional groups, the nanotube structural integrity and conductivity can be maintained which are desirable characteristics of electrocatalysts. This eliminates over-oxidation and the introduction of less-desired functional groups which can be an issue with graphene oxide-based catalysts.

Metal impurities introduced during carbon nanotube synthesis or during electrocatalyst preparation should also be considered as factors that affect ORR activity since impurities

are often considered as the possible active center for ORR,[2,6] but this is still under dispute.[2,10] To characterize the amount of remaining impurities, ICP-MS analysis (Table 1) indicated an extremely low amounts of Fe and Co for DMWNT-H_2SO_4 and even lower amounts for DMWNT-HNO_3. Furthermore, although limited to the surface, XPS results (Fig. S11) for DMWNT-H_2SO_4 following annealing in Ar at 900°C (DMWNT-H_2SO_4-Ar900) shows no detectable Co or N. These results indicate that acid washing after drilling was successful in removing the overwhelming majority of residual metals.

Table 1. Characterizations of residual metal impurities by inductively coupled plasma mass spectrometry (ICP-MS)

Sample	Fe wt%	Co wt%	Fe at%	Co at%
DMWNT-HNO_3	0.006	0.0045	0.0013	0.00091
DMWNT-H_2SO_4	0.083	0.055	0.018	0.011
DMWNT-H_2SO_4-Ar900	0.015	0.0032	0.0027	0.00065
(After electrochemical characterizations)				

Weight percent and atomic percent of DMWNT-HNO_3 and DMWNT-H_2SO_4 samples from ICP-MS measurements. DMWNT-H_2SO_4-Ar900 denotes sample that was annealed in Ar at 900˚C.

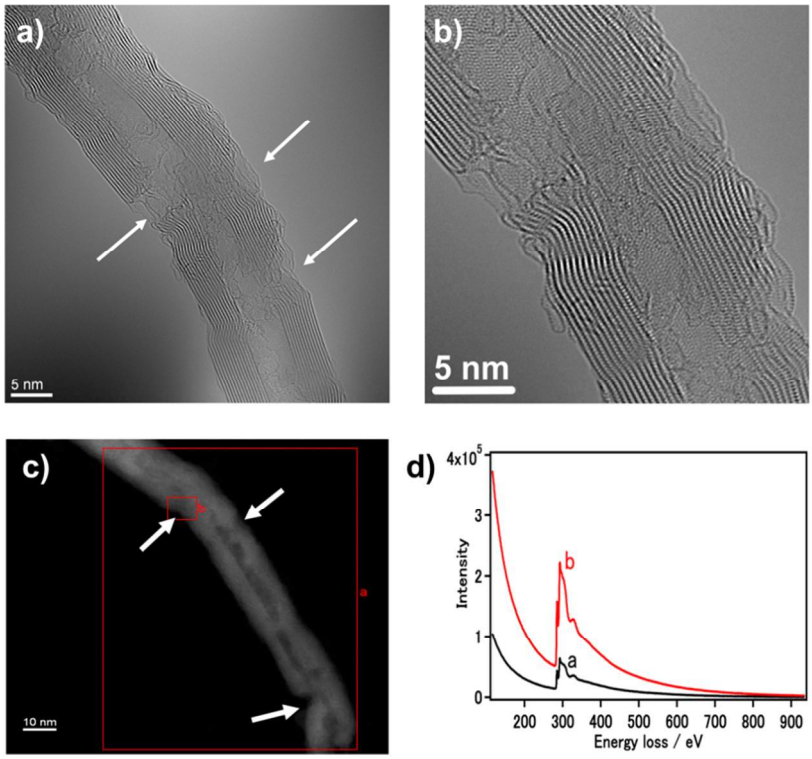

Fig. 5 Monochromated TEM images of DMWNT-H_2SO_4 annealed at 900°C in Ar (DMWNT-H_2SO_4-Ar900) following ORR electrochemical characterizations (a) showing the distinct induced drilled defects (b) close up showing closer view of the drilled holes and edge defects (c) HAADF image of the same vicinity with smaller magnification (d) EELS spectrum summed over the indicated areas labeled a, b taken from (c). The arrows indicate the locations of chemically drilled hole defects.

While the source of improved activity in DMWNT-H_2SO_4-Ar900 is possibly related to its higher amount of impurities, the differences in defect morphology cannot be overlooked. One of the advantages of using bulk and free standing buckypaper is the ability to characterize the level of impurities before and after electrochemical characterizations without any sample loss. Interestingly, DMWNT-H_2SO_4-Ar900 after ORR characterizations showed significantly lower Fe and Co impurities in comparison to DMWNT-H_2SO_4 before ORR characterizations (Table 1) without any differences in ORR performance. In contrast, typical studies involving transition metal catalysts report an optimal metal content of 0.2-4 wt%.[2,6] While the dissolution of impurities after CV cycling can be expected, to the best of our knowledge, there has been no previous report on the examination of the level of impurities after electrochemical characterizations. For the most active sample, (DMWNT-H_2SO_4-Ar900, after electrochemical characterizations), since the amount of impurities decreases by one order in the magnitude (Table 1), it is concluded that it is unlikely that impurities directly

contribute towards ORR and thus it is suggested that carbon restructuring and the possible formation of topological pentagon/heptagon defects is a reasonable explanation for the enhanced activity in our non-nitrogen doped and non-metal carbon nanotube-based catalysts. Additionally, we have studied the effect of impurities in the MWNTs, originating from the production process (Fe impurity). With the same annealing process, pristine (raw) MWNT-Ar900 showed much lower ORR activity than that of DMWNT-H_2SO_4-Ar900. This also suggests that impurities themselves are not the key for the high ORR activity in our catalysts (Fig. S12). Lastly, we have also conducted a durability test (Fig. S13) of DMWNT-H_2SO_4-Ar900. The CV results before and after durability test show the degradation of ORR activity, which is believed to be related to a reduction of active sites. Interestingly, the results also indicate that re-annealing at 900°C in Ar of the sample after the durability test shows a significant recovery in ORR activity. These findings further supports that it is unlikely that impurities contribute to the ORR. To the best of our knowledge, such recovery of ORR activity after re-annealing has not been reported and this is made possible by the utilization of buckypaper. It has been suggested, however, that while the presence of metals may not directly contribute to ORR, it is possible that metals may catalyze the formation of ORR beneficial defect sites.[29] To further investigate the structure of the disordered surfaces and edges, monochromated TEM, HAADF-STEM imaging, and STEM-EELS measurements were conducted. Monochromated TEM (Fig. 5a,b) of DMWNT-H_2SO_4-Ar900 sample after ORR characterizations shows the well-defined drilled hole defects and the intact walls which maintains high crystallinity. The HAADF image (Fig. 5c) further confirms the presence of hole defects since the intensity is sensitive to the atomic number Z and as result, the hole defect area becomes darker. Additionally, there are no specific bright spots indicating that heavy elements and impurities are absent. EELS analysis (Fig. 5d) on the enclosed areas labeled a, b indicates only pure carbon. From all of the detailed analysis of impurities, it can be concluded that the active sites are unlikely metal-carbon coordinated complexes.

With respect to the possible location of the active sites, Jaouen et al. have reported that microporosity formed after the carbon etching by NH_3 annealing may act as the host for active site-Fe/N complex.[30] In order to clarify whether the micropores are correlated to the high ORR activity of our catalysts, t-plot analyses have been conducted for DMWNT-H_2SO_4 and DMWNT-H_2SO_4-Ar900 (Fig. S14). The linear region passing through the origin, suggests the absence of micropores in our catalysts. With the absence of such microporosity, we can conclude that the micropores formation is not essential to our catalysts.

To further confirm the ORR characterizations to actual fuel cell conditions, single cell testing was performed with DMWNT-H_2SO_4 annealed at 900°C in Ar (DMWNT-H_2SO_4-Ar900) catalyst. The fuel cell polarization and power density curves (Fig. 6) shows that the cell generates an OCV of 0.74 V and the maximum output power obtained was 103 mW cm^{-2} at the voltage of 0.23 V and current of 450 mA cm^{-2}. As a reference, Ozaki and coworkers with transition metal and nitrogen-doped nanoshell carbons[4] also called carbon alloys,[31] reported a similar OCV at 0.78 V, and a maximum power density of 210 mW cm^{-2}, but with a cathode catalyst loading (3.8 mg cm^{-2}) that is double of our setup (1.85 mg cm^{-2}). [4] When normalized to mass (55.68 mW mg^{-1}), our catalyst exhibits similar power generation performance. This shows that our non-nitrogen doped and non-metal carbon-based catalyst in a single fuel cell setup is competitive when compared with transition metal and nitrogen doped carbons.

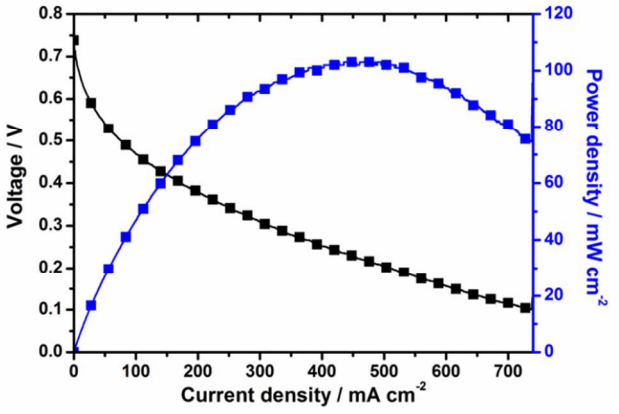

Fig. 6 Single cell containing DMWNT-H_2SO_4 after Ar heat treatment at 900°C (DMWNT-H_2SO_4-Ar900). Cell temperature: 90°C, anode gas: pure hydrogen (200 sccm, 0.3 MPa), cathode gas: pure oxygen (400 sccm, 0.3 MPa). The catalyst loading is 1.85 mg cm^{-2} for cathode and 1 mg cm^{-2} of Pt/C (70 wt%) for anode.

We do acknowledge that by using our buckypaper setup, we are unable to rotate the electrode to give additional information on the ORR mechanism. Conventional rotating disk electrode (RDE) based characterization techniques that employ drop-casting suffers from potential discrepancies in catalyst dispersion and mass loading, which leads to issues with reproducibility because our pure carbon catalyst exhibits low wettability in solution. Photographs of RDEs loaded with some of our samples (Fig. S15), illustrates the issues we encountered with dispersion and mass loading. This is possibly due to poor wettability of the inert basal plane of the intact inner tubes and results in an uneven film when loaded on the RDE, even though the prepared catalyst ink of Nafion/water/ethanol solution appears homogeneous. Attempting to calculate the electron number (n_e) partaking in the reaction for DMWNT-H_2SO4-Ar900, an alternative RDE preparation technique was applied to characterize the n_e. As discussed earlier, the main challenge for drop casted RDEs is the preparation of a uniform surface with consistent mass loading especially for samples with very poor wettability, such as carbon without any oxygen functionalities. Thus, for analyzing the DMWNT-H_2SO4-Ar900, instead of removing the functional groups followed by preparation of ink solution, we drop casted DMWNT-H_2SO_4 (containing functional

groups) on a detachable glassy carbon (GC) disk electrode, followed by annealing the drop casted GC disk under Ar atmosphere at 900 °C, for 1 hour forming a uniform sample loading (Fig. S15). The ORR polarization curves and Koutecky-Levich plots of DMWNT-H_2SO4-Ar900 (Fig. S16) suggests that our catalyst favors the 2-electron indirect ORR pathway via peroxide formation, despite the enhancement of the onset potential up to 0.73 V and supported with comparable power generation performance to nitrogen doped carbon alloys.[4]

Conclusions

By investigating the origin of high ORR activity in non-nitrogen doped and non-metal catalysts based on chemically-drilled MWNTs, new insights are gained between the roles of oxygen functionalities, defect structure, and impurities. Through ORR characterizations and TPD analysis, the availability of new active sites occurs after annealing at 500°C and higher. The new active sites are correlated to the removal of high temperature CO desorbing functional groups, changes in morphology, and the possible formation of topological defects from carbon restructuring. The results suggest that the direct contribution of impurities towards ORR is unlikely due to the very low amount of detectable residual metals from ICP-MS, and the absence of metal-carbon coordination from the HAADF-STEM and STEM-EELS measurements of the sample after electrochemical characterizations without any changes in ORR performance during the measurement. For further confirmation, a fuel cell with a catalyst loading of 1.85 mg cm^{-2} containing the most active sample, DMWNT-H_2SO_4 after annealing at 900°C in Ar, was tested and resulted in an OCV of 0.74 V and maximum power density of 113.5 mW mg^{-1}. It should be noted that with our chemical drilling method and the introduction of 5.30 at% of oxygen (Table S1), containing 4.12 at% of oxygen from CO desorbing functional groups, the initiation of high ORR activity was attained. This eliminates unnecessary over-oxidation which introduces less-desirable functional groups and can damage and reduce the crystalinity and conductivity of the carbon material. Our results provide important insights for designing carbon-based ORR catalysts.

Acknowledgements

The authors would like to acknowledge and thank Mr. Hiroshi Watanabe for assistance with the experimental work, Mr. Shinpei Nakamura for the ICP-MS analysis, and Dr. Daling Lu for the FE-TEM analysis. The authors also thank Showa Denko KK for providing the carbon nanotubes used in this work and for carrying out the fuel cell test. This work is funded by the Japan Science and Technology Agency (JST). Their contribution is greatly appreciated. This work is also supported by the Nanotechnology Platform by MEXT of Japan.

Notes and references

[†]*Department of Energy Sciences, Tokyo Institute of Technology, 4259 Nagatsuta-cho, Midori-ku, Yokohama-shi 226-8502, Japan*
[§]*National Institute for Materials Science, 1-1 Namiki, Tsukuba, Ibaraki 305-0044, Japan*
[‡]*Center for Low Carbon Society Strategy, Japan Science and Technology Agency, 7, Gobancho, Chiyoda-ku, Tokyo 102-0076, Japan*
Corresponding Author
* waki.k.aa@m.titech.ac.jp

Electronic Supplementary Information (ESI) available: [Double layer normalization, TPD quantitative characterizations, supplementary Fig. S1-S11]. See DOI: 10.1039/b000000x/

1. Z. Chen, D. Higgins, A. Yu, L. Zhang and J. Zhang, *Energy Environ. Sci*,. 2011, **4**, 3167−3192.
2. C. W. B. Bezerra, L. Zhang, K. C. Lee, H. S. Liu, A. L. B. Marques, E. P. Marques, H. J. Wang and J. J. Zhang, *Electrochim. Acta*, 2008, **53**, 4937−4951.
3. R. Jasinski, *Nature*, 1964, **201**, 1212.
4. J. Ozaki, S. Tanifuji, A. Furuichi and K. Yabutsuka, *Electrochim. Acta*, 2010, **55**, 1864−1871.
5. H. R. Byon, J. Suntivich, E. J. Crumlin and Y. Shao-Horn, *Phys. Chem. Chem. Phys.*, 2011, **13**, 21437-21445.
6. Y. Li, W. Zhou, H. Wang, L. Xie, Y. Liang, F. Wei, J-C. Idrobo, S. J. Pennycook and H. Dai, *Nat. Nanotechnol.*, 2012, **7**, 394−400.
7. R. Yang, K. Stevens and J. R. Dahn, *J. Electrochem. Soc.*, 2008, **155(1)**, B79-B91.
8. K. P. Gong, F. Du, Z. H. Xia, M. Durstock and L. M. Dai, *Science*, 2009, **323**, 760–764.
9. S. Y. Wang, D. S. Yu and L. M. Dai, *J. Am. Chem. Soc.*, 2011, **133**, 5182–5185.
10. M. Kobayashi, H. Niwa, Y. Harada, K. Horiba, M. Oshima, H. Ofuchi, K. Terakura, T. Ikeda, Y. Koshigoe, J. Ozaki, S. Miyata, S. Ueda, Y. Yamashita, H. Yoshikawa and K. Kobayashi, *J. Power Sources*, 2011, **196**, 8346–8351.
11. F. Charreteur, F. Jaouen, S. Ruggeri and J. Dodelet, *Electrochim. Acta*, 2008, **53**, 2925–2938.
12. I. Kruusenberg, N. Alexeyeva, K. Tammeveski, J. Kozlova, L. Matisen, V. Sammelselg, J. Solla-Gullon and J. M. Feliu, *Carbon*, 2011, **49**, 4031–4039.
13. S. Kundu, T. C. Nagaiah, W. Xia, Y. M. Wang, S. Van Dommele, J. H. Bitter, M. Santa, G. Grundmeier, M. Bron, W. Schuhmann and M. J. Muhler, *Phys. Chem. C*, 2009, **113**, 14302–14310.
14. R. Kannan, U. Bipinlal, S. Kurungot and V. K. Pillai, *Phys. Chem. Chem. Phys.*, 2011, **13**, 10312–10317.
15. P. J. Britto, K. S. V. Santhanam, A. Rubio, J. A. A. Alonso and P. M. Ajayan, *Adv. Mater.*, 1999, **11**, 154–157.
16. K. Matsubara and K. Waki, *Electrochim. Acta*, 2010, **55 (28)**, 9166−9173.
17. K. Matsubara and K. Waki, *Electrochem. Solid-State Lett.*, 2010, **13**, F7–F9.
18. H. S. Oktaviano, K. Yamada and K. Waki, *J. Mater. Chem.*, 2012, **22**, 25167–25173.

19. D-H. Kim and K. Waki, *J. Nanosci. Nanotechnol.*, 2010, **10**, 2375–2380.
20. J. L. Figuereido, M. F. R. Pereira, M. M. A. Freitas and J. J. M. Orfao, *Carbon*, 1999, **37(9)**, 1379–1389.
21. S. Kundu, Y. Wang, W. Xia and M. Muhler, *J. Phys. Chem. C*, 2008, **112**, 16869-16878.
22. H-H. Yang and R. L. McCreery, *J. Electrochem. Soc.*, 2000, **147(9)**, 3420-3428.
23. I. Kruusenberg, N. Alexeyeva and K. Tammeveski, *Carbon*, 2009, **47**, 651–658.
24. M. Hara, *Energy Environ Sci.* 2010, **3**, 7936-7942.
25. T. Sharifi, G. Hu, X. Jia and T. Wagberg, *ACS Nano*, 2012, **6**, 8904-8912.
26. E. J. Biddinger and U. S. Ozkan, *J. Phys. Chem. C*, 2010, **114**, 15306–15314.
27. T. Fujimori, K. Urita, T. Ohba, H. Kanoh and K. Kaneko, *J. Am. Chem. Soc.* 2010, **132**, 6764-6767.
28. J. M. Leyssale, J. P. Da Costa, C. Germain, P. Weisbecker and G. L. Vignoles, *Carbon*, 2012, **50**, 4388-4400.
29. P. H. Matter, L. Zhang and U. S. Ozkan, *J. Catal.*, 2006, **239**, 83–96.
30. F. Jaouen, M. Lefevre, J-P. Dodelet, M. Cai, *J. Phys. Chem. B*, 2006, **110**, 5553-5558.
31. T. Ikeda, M. Boero, S. F. Huang, K. Terakura, M. Oshima and J. Ozaki, *J. Phys. Chem. C*, 2008, **112**, 14706–14709.